Of note, food intake was not significantly altered in these mice, suggesting that changes in fat mass were likely due to increased energy expenditure (fig. S12B). Consistent with the body-weight reduction, serum leptin levels were also significantly reduced (Fig. 3C).

The db/db mutant mice display a characteristic dysregulation of blood glucose and serum insulin levels, and we studied whether the hypothalamic cell transplantation corrected these metabolic abnormalties. In comparison with controls, hypothalamically chimeric db/db mice displayed a large and significant reduction of blood glucose levels at both 9 and 13 weeks after transplantation (Fig. 3D), consistent with the known central role of hypothalamic leptin receptors in peripheral glucose regulation (34). Interestingly, this rescue of peripheral glucose homeostasis occurred despite the lack of difference in serum insulin relative to controls (fig. S12C).

These results demonstrate that transplanted newborn hypothalamic neurons and progenitors of appropriate developmental stage can chimerically integrate into hypothalamic circuitry as functional neurons with subtype diversity typical of the normal hypothalamus, and that this relatively small number of functionally integrated donor neurons can ameliorate obesity, hyperleptinemia, and hyperglycemia in db/db mice. At least two possible network mechanisms might explain how the relatively few integrated neurons partially rescue the db/db phenotype. Rescue might be solely due to the new neurons themselves. Alternatively, the new, cell-autonomously leptin-responsive neurons might modulate their firing in response to systemic leptin levels, secondarily regulating other neurons in hypothalamic circuitry. Thus, transplanted neurons might act as leptin sensors whose output is then transmitted by endogenous, hypothalamic circuitry still unresponsive to direct leptin activation. Irrespective of the underlying mechanism, these experiments demonstrate that synaptic integration by leptin-responsive donor neurons can impart an organism-level rescue of metabolic defects, thereby providing a proof of concept for cell-mediated repair of a neuronal circuit controlling a complex phenotype.

References and Notes

1. J. M. Friedman, J. L. Halaas, *Nature* **395**, 763 (1998).
2. J. S. Flier, *Cell* **116**, 337 (2004).
3. P. Cohen *et al.*, *J. Clin. Invest.* **108**, 1113 (2001).
4. T. J. Kowalski, S. M. Liu, R. L. Leibel, S. C. Chua Jr., *Diabetes* **50**, 425 (2001).
5. M. V. Kokoeva, H. Yin, J. S. Flier, *Science* **310**, 679 (2005).
6. M. V. Kokoeva, H. Yin, J. S. Flier, *J. Comp. Neurol.* **505**, 209 (2007).
7. E. van de Wall *et al.*, *Endocrinology* **149**, 1773 (2008).
8. Materials and methods are available as supporting material on *Science* Online.
9. P. H. Ozdinler, J. D. Macklis, *Nat. Neurosci.* **9**, 1371 (2006).
10. C. S. Hernit-Grant, J. D. Macklis, *Exp. Neurol.* **139**, 131 (1996).
11. J. J. Shin *et al.*, *J. Neurosci.* **20**, 7404 (2000).
12. R. A. Fricker-Gates, J. J. Shin, C. C. Tai, L. A. Catapano, J. D. Macklis, *J. Neurosci.* **22**, 4045 (2002).
13. C. Scharff, J. R. Kirn, M. Grossman, J. D. Macklis, F. Nottebohm, *Neuron* **25**, 481 (2000).
14. H. van Praag *et al.*, *Nature* **415**, 1030 (2002).
15. U. S. Sohur, J. G. Emsley, B. D. Mitchell, J. D. Macklis, *Philos. Trans. R. Soc. Lond. B Biol. Sci.* **361**, 1477 (2006).
16. D. E. McNay, M. Pelling, S. Claxton, F. Guillemot, S. L. Ang, *Mol. Endocrinol.* **20**, 1623 (2006).
17. M. Shimada, T. Nakamura, *Exp. Neurol.* **41**, 163 (1973).
18. S. L. Padilla, J. S. Carmody, L. M. Zeltser, *Nat. Med.* **16**, 403 (2010).
19. Y. D. Zhou *et al.*, *Nat. Med.* **15**, 1208 (2009).
20. D. Burdakov, F. M. Ashcroft, *J. Neurosci.* **22**, 6380 (2002).
21. T. Miki *et al.*, *Nat. Neurosci.* **4**, 507 (2001).
22. Y. H. Jo, D. Wiedl, L. W. Role, *J. Neurosci.* **25**, 11133 (2005).
23. N. Ibrahim *et al.*, *Endocrinology* **144**, 1331 (2003).
24. S. H. Bates *et al.*, *Nature* **421**, 856 (2003).
25. H. Münzberg, L. Huo, E. A. Nillni, A. N. Hollenberg, C. Bjørbaek, *Endocrinology* **144**, 2121 (2003).
26. C. Li, J. M. Friedman, *Proc. Natl. Acad. Sci. U.S.A.* **96**, 9677 (1999).
27. M. A. Cowley *et al.*, *Nature* **411**, 480 (2001).
28. M. van den Top, K. Lee, A. D. Whyment, A. M. Blanks, D. Spanswick, *Nat. Neurosci.* **7**, 493 (2004).
29. M. Claret *et al.*, *J. Clin. Invest.* **117**, 2325 (2007).
30. L. E. Parton *et al.*, *Nature* **449**, 228 (2007).
31. X. Fioramonti *et al.*, *Diabetes* **56**, 1219 (2007).
32. S. A. Bayer, J. Altman, *Neocortical Development* (Raven Press, New York, 1991).
33. H. Dhillon *et al.*, *Neuron* **49**, 191 (2006).
34. J. W. Hill *et al.*, *Cell Metab.* **11**, 286 (2010).

Polarization of PAR Proteins by Advective Triggering of a Pattern-Forming System

Nathan W. Goehring,[1] Philipp Khuc Trong,[2,1]* Justin S. Bois,[2,1]† Debanjan Chowdhury,[2]‡ Ernesto M. Nicola,[2]§ Anthony A. Hyman,[1] Stephan W. Grill[2,1]‖

In the *Caenorhabditis elegans* zygote, a conserved network of partitioning-defective (PAR) polarity proteins segregates into an anterior and a posterior domain, facilitated by flows of the cortical actomyosin meshwork. The physical mechanisms by which stable asymmetric PAR distributions arise from transient cortical flows remain unclear. We present evidence that PAR polarity arises from coupling of advective transport by the flowing cell cortex to a multistable PAR reaction-diffusion system. By inducing transient PAR segregation, advection serves as a mechanical trigger for the formation of a PAR pattern within an otherwise stably unpolarized system. We suggest that passive advective transport in an active and flowing material may be a general mechanism for mechanochemical pattern formation in developmental systems.

Developmental form emerges from coupling of pattern-forming biochemical networks with mechanical processes (1–3).

In *Caenorhabditis elegans* zygotes, transient flows of a thin film of a mechanically active actomyosin cell cortex instruct the patterning of a conserved cell polarity pathway consisting of two groups of partitioning-defective (PAR) proteins that mutually exclude one another from the cell membrane (4–14). Initially, anterior PARs (aPARs: PAR-3, PAR-6, and atypical protein kinase C) cover the entire cell membrane. During polarization, flows of cortical actomyosin oriented away from the posterior-localized centrosome induces

[1]Max Planck Institute of Molecular Cell Biology and Genetics (MPI-CBG), 01307 Dresden, Germany. [2]Max Planck Institute for the Physics of Complex Systems (MPI-PKS), 01187 Dresden, Germany.

*Present address: Department of Physics, and Department of Applied Mathematics and Theoretical Physics, University of Cambridge, Cambridge CB3 OHE, UK.
†Present address: Department of Chemistry and Biochemistry, University of California, Los Angeles, Los Angeles, CA 90095, USA.
‡Present address: Department of Physics, Harvard University, Cambridge, MA 02138, USA.
§Present address: Institute for Cross-Disciplinary Physics and Complex Systems (IFISC), Consejo Superior de Investigaciones Científicas–Universitat de les Illes Balears, E-07122 Palma de Mallorca, Spain.
‖To whom correspondence should be addressed. E-mail: grill@mpi-cbg.de

the segregation of aPARs, accompanied by formation of a domain of posterior PARs (pPARs: PAR-1, PAR-2, and LGL) (*10*, *15*). Flows then cease, but the domains remain (*16*).

The physical mechanism by which flows induce segregation of aPARs is unclear. Consideration of the actomyosin cortex as a thin film of an active fluid (*14*) raises the possibility of passive advective transport of fluid-embedded molecules by the flowing cell cortex. Whether fluid flow advects entrained molecules depends on both their diffusivity and the flow velocities to which they are subjected. The relative contributions of advection and diffusion can be assessed by a dimensionless Péclet number (*Pe*), defined as the ratio of a diffusive to an advective time scale. We estimate that *Pe* is of order unity for both PAR-2 (*Pe* ≈ 3) and PAR-6 (*Pe* ≈ 2.5) (*10*, *17*, *18*) [supporting online material (SOM) text 2.1]. Thus, cortical flows are fast enough and PAR proteins are membrane-associated long enough that advection should affect their distribution as they diffuse on the membrane.

We next asked whether advection can account for the segregation of PAR-6 observed in embryos depleted of pPAR protein PAR-2. Here, aPARs segregate in response to flows but remain segregated only as long as flows persist (*10*, *16*) (Fig. 1D). In this regime, the behavior of aPARs on the membrane can be described by a combination of lateral diffusion, spontaneous membrane binding and unbinding (*18*), and advection by flow. Assuming that membrane association follows simple mass action kinetics, the local aPAR concentration $A(x,t)$ at time t and position x on the membrane is given by

$$\partial_t A = D_A \partial_x^2 A - \partial_x(vA) + k_{on,A}A_{cyto} - k_{off,A}A \tag{1}$$

where D_A is the diffusivity of aPARs in the membrane-bound state, $v(x,t)$ is the cortical flow velocity, $k_{on,A}$ and $k_{off,A}$ are the respective coefficients for membrane association and dissociation of aPAR, and A_{cyto} is the uniform cytoplasmic concentration, for which we assume rapid mixing (*18*). Because the total amount of aPAR appears to be conserved, A_{cyto} is given by the total aPAR amount minus that associated with the membrane (SOM text 2.2). By using measured parameters (*18*) (table S1 and SOM text 1.4) and cortical flow velocities determined in embryos depleted of PAR-2 (fig. S1A), we calculated the impact of flow on an initially homogeneous aPAR distribution. This reproduced the pattern of PAR-6 segregation observed in embryos depleted of PAR-2 (Fig. 1), suggesting that advection by fluid flow is sufficient to displace aPARs transiently.

Because advection-based segregation persists only as long as flow velocities remain sufficiently high, how does transient flow yield stable polarization? In vivo, this requires both species (*4–6*). PAR-2 behaves similarly to PAR-6 (*18*) and can be described analogously to Eq. 1 to give

$$\partial_t A = D_A \partial_x^2 A - \partial_x(vA) + R_A$$
$$\partial_t P = D_P \partial_x^2 P - \partial_x(vP) + R_P \tag{2}$$

where P is the local membrane concentration of pPARs, D_P denotes the diffusivity of membrane-bound pPARs, and R_A and R_P denote the reaction terms that describe membrane association and dissociation that now include interactions between the two species. We include reciprocal antagonistic feedback as detachment that depends on the concentration of the opposing species (Fig. 2A). Importantly, if this feedback is sufficiently nonlinear, mutual antagonism between A and P endows the system with a bistable character such that the membrane will tend to exist in one of two states: an anterior-like state, with $A > P$, or a posterior-like state with $A < P$ (see below) (*19*). Therefore,

$$R_A = k_{on,A}A_{cyto} - k_{off,A}A - k_{AP}P^\alpha A$$
$$R_P = k_{on,P}P_{cyto} - k_{off,P}P - k_{PA}A^\beta P \tag{3}$$

where k_{AP} is a coefficient governing antagonism of A by P with α specifying stoichiometry and k_{PA} and β are similarly defined; $k_{on,P}$, $k_{off,P}$, and P_{cyto} are analogous to the corresponding A-specific variables. A similar framework without bistable character was proposed in (*20*), instead requiring local effects of the actin cortex on aPAR association rates for pattern formation.

Bistability in the reaction terms (Fig. 2B) has two important consequences that allow the system to account simultaneously for the unpolarized and polarized states of the embryo. First, bistability can drive the entire membrane of the system into one of two states: either an anterior-like homogeneous state, with aPARs enriched in the membrane and pPARs in the cytoplasm (similar to the *C. elegans* embryo before polarization), or the analogous posterior-like homogeneous state. Second, bistability also permits the system to support coexistence of distinct membrane domains in opposite states, separated in space and connected by boundary regions. A polarized system would contain exactly two such domains.
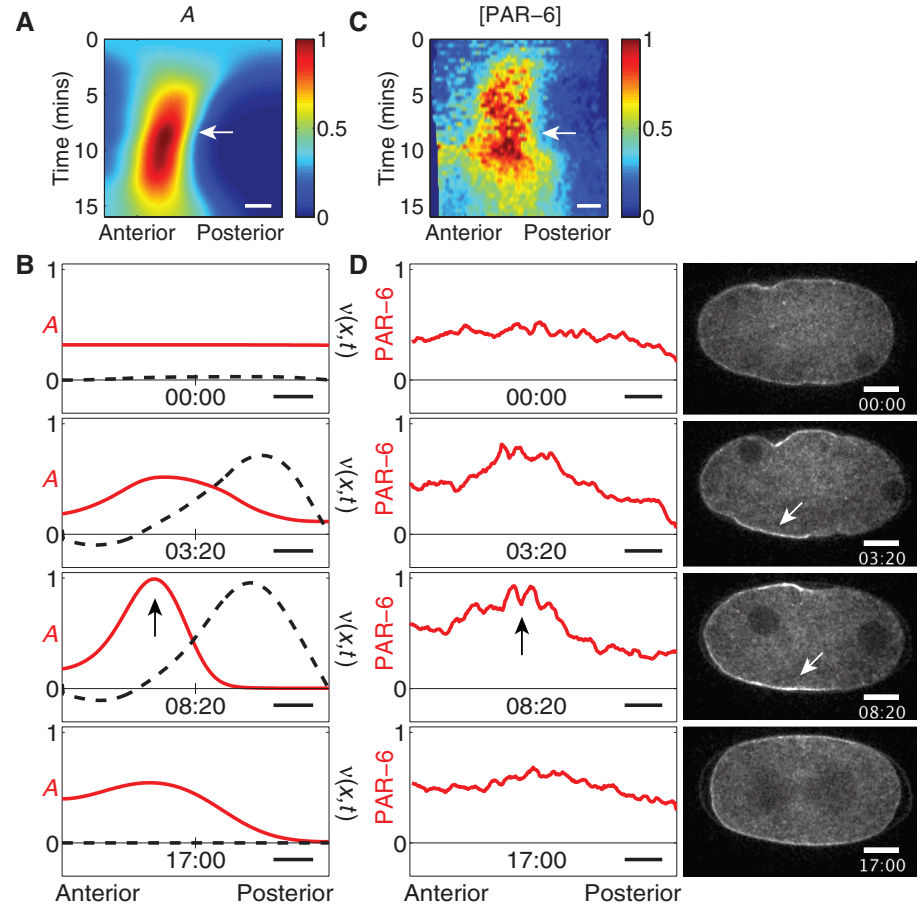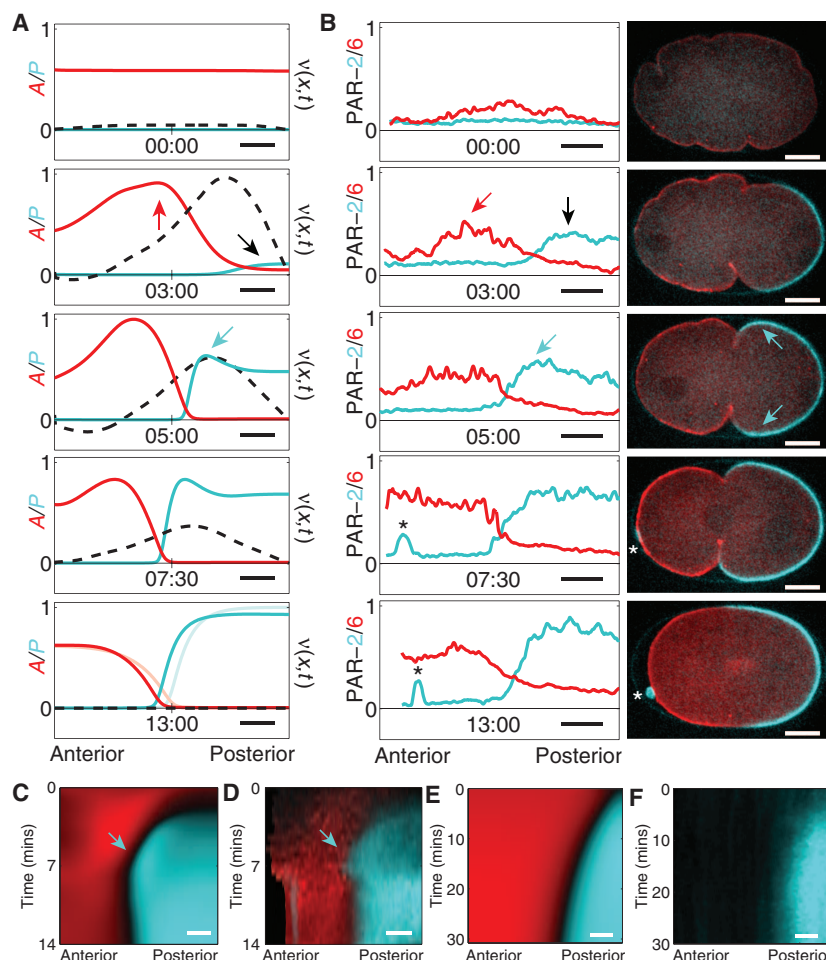
Fig. 1. Advection drives transient anterior displacement of PAR-6 in *par-2(RNAi)* embryos. (**A**) Calculated kymograph of *A* over time when subject to the measured flow profile (movie S1). (**B**) *A* (red) and the instantaneous flow velocity (*v*, dashed black) at selected times. Positive velocity indicates flow toward the anterior. (**C**) Kymograph of GFP::PAR-6 distributions. (**D**) GFP::PAR-6 fluorescence profiles (left) and the corresponding images from movie S2 (right). Arrows indicate regions of aPAR enrichment just beyond midcell. We show an average of the upper and lower PAR-6 profiles along the membrane and half of the spatial system for *A*. Values are normalized to the maximum values of *A* and PAR-6, respectively. Time (min:s). Scale bars indicate 10 μm.
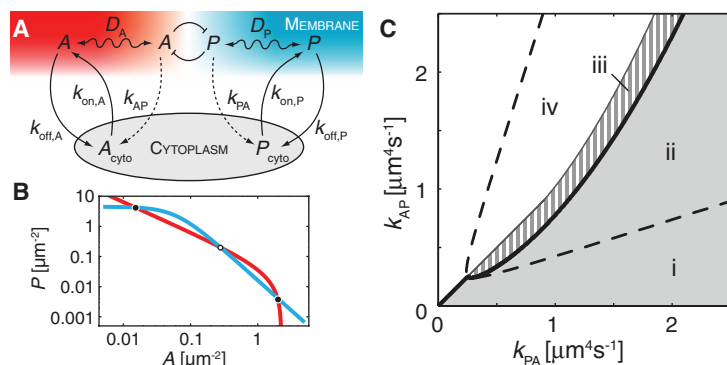
Fig. 2. Features of the reaction-diffusion PAR model. (**A**) PARs exchange (arrows) between a well-mixed cytoplasm and a membrane-associated state, where they diffuse laterally (wavy arrows) and are subject to detachment by antagonism (dashed arrows). (**B**) Nullclines of solutions to Eq. 3 (*A*, red; *P*, blue) for fixed cytosolic concentrations $A_{cyto} = 1.42\ \mu m^{-3}$ and $P_{cyto} = 0.69\ \mu m^{-3}$. The three intersections reflect the real, positive fixed-point solutions; the outer two are stable (solid circles). (**C**) Regions of parameter space defined by k_{AP} and k_{PA}. Homogeneous aPAR-dominant states exist within the shaded region, where they are linearly stable, and within the cross-hatched region, where they are unstable. The dashed line encloses the region permitting stable polarized states (regions ii, iii, and iv). In region i, the homogeneous aPAR-dominant state is stable but does not coexist with a polarized solution. In region ii, both homogeneous aPAR-dominant and polarized steady states exist and are stable. Here, polarization requires perturbation beyond a threshold. In region iii, both states exist, but the homogeneous aPAR-dominant state is unstable. In region iv, a homogeneous aPAR-dominant state does not exist. An illustrative parameter set is used to emphasize topology and relevant features (SOM text 1.4). See fig. S2A for measured *C. elegans* parameters.

Examination of the parameter space defined by k_{AP} and k_{PA} in the absence of flow for regimes permitting bistability (SOM text 2.3) reveals a multistable character (Fig. 2C and fig. S2), with regions permitting stable polarized solutions overlapping those permitting a stable homogeneous anterior-like state (Fig. 2C, ii). Here, the system displays hysteresis, and the transition from the unpolarized anterior-like state to a polarized state is possible only through application of a perturbation that exceeds a critical size. This "threshold" behavior ensures that the system will not polarize in response to small fluctuations, which could otherwise lead to inappropriate timing or geometry of the resulting asymmetric cell division. Once it does polarize, it remains so even after the polarity-inducing signal is no longer active, similar to what is seen in the embryo (*15*).

Because cortical flows can displace aPARs from the posterior, they might provide a sufficient perturbation to trigger polarization. To test this, we selected a parameter regime that permits both a stable polarized and a stable anterior-like unpolarized state (table S1) and subjected a system in the latter state to flow as measured in wild-type embryos (fig. S1B). At the onset of flow, aPARs were segregated toward the anterior as

Fig. 3. Advection provides a robust polarity trigger. (**A**) Calculated *A* (red) and *P* (cyan) profiles with the homogeneous aPAR-dominant state subject to measured wild-type (WT) flow velocities (dashed black line; positive velocities are toward the anterior; see movie S3). Shaded lines in last time point indicate steady-state distributions. (**B**) GFP::PAR-6 (red) and mCherry::PAR-2 (cyan) fluorescence profiles (left) and still images from movie S4 (right). Red arrows indicate aPAR enrichment by advection, cyan arrows indicate leading edge enrichment of pPARs, and black arrows indicate nascent pPAR domains. The small PAR-2 peak in the anterior (*) is due to the polar body. (**C** and **D**) Kymographs of (A) and (B), with *A*/PAR-6 in red and *P*/PAR-2 in cyan. (**E**) Slow polarization in the model in a no-flow regime with triggering by local aPAR reduction (fig. S4A). (**F**) Slow polarization in vivo in a no-flow regime. PAR-6 is not shown. Still images in fig. S5. Note the difference in scaling of time on the *y* axis in (C) and (D) versus (E) and (F). Time (min:s). Scale bars indicate 10 μm.

in the aPAR-only system (Fig. 3, A and C). However, with the posterior species present, the reduction of aPARs in the posterior allowed formation of a small pPAR domain, which grows to reach its maximal size in less than 10 min. This pattern of polarization recapitulated measurements of wild-type embryos undergoing polarization, reproducing not only the final steady-state PAR distributions (fig. S3, A and B) but also the leading-edge enrichment, and the initial overexpansion of the growing pPAR domain before relaxation to steady state once flows attenuated (Fig. 3, B and D).

To examine whether the observed spatio-temporal patterns of PAR redistribution were due to flows, we examined polarization in a no-flow regime. Note that polarization in the model is insensitive to the precise form of the trigger, provided that it induces a sufficiently large perturbation of the unpolarized state. However, the spatiotemporal evolution of PAR distributions will depend substantially on the type of trigger. We examined the evolution of an aPAR-dominant state with aPAR locally reduced at the posterior pole, which polarizes in the absence of flow (fig. S4A). We obtained neither the characteristic shapes of PAR distributions during the onset phase nor the typical overexpansion of the posterior domain beyond midcell (compare Fig. 3E versus C and D). Moreover, the time required to polarize, here defined as the pPAR domain reaching 95% of its steady-state size, exceeds 40 min in simulations (Figs. 3E and 4B). In vivo, a similar situation is seen in embryos polarizing through a "rescue" pathway, which allows embryos lacking normal cortical flows to form PAR-2 domains, albeit domains that form later and fail to reach full size (21–23). Here, triggering likely occurs through local cues that stimulate or inhibit membrane-association of PAR species (23). We found that such embryos exhibited slowed domain growth and lacked both leading-edge enrichment of PAR-2 and the initial overexpansion of the growing posterior domain (Fig. 3F and fig. S5), indicating that the observed spatiotemporal patterns of PAR redistribution are specifically due to flows.

Given that PAR distributions in the polarized steady state are not determined by the type and form of the trigger, we next asked how the steady state is determined. Evolution to steady state occurs through a front-stalling behavior that is similar to a model for polarization of Rho-family guanosine triphosphatases (GTPases) (fig. S4, A, D, and E) (19). Stalling relies on depletion of a cytoplasmic pool, which, given conserved protein amounts, couples domain growth to a global reduction in membrane association (fig. S4F) (24). Similar roles for limiting pools have been proposed in other cell polarity systems (25–27).

This central role of limiting pools in constraining domain expansion makes two key predictions. First, domain growth should be directly coupled to depletion of the cytoplasmic pool (Fig. 4, A and B). Indeed, monitoring cytoplas-

mic fluorescence of PAR-2 during polarization revealed that cytoplasmic depletion and domain growth are coupled (Fig. 4C). Second, changing the amount of a given PAR protein should result in changes in the steady-state position of the PAR boundary (fig. S6). We found that PAR-2 domains were larger in embryos possessing only one functional *par-6* gene copy (Fig. 4, D and E) and in embryos where PAR-2 was overexpressed by optimizing the codon adaptation index (CAI) of the green fluorescent protein *(gfp)::par-2* transgene (Fig. 4, F to H) (28). Similarly, partial depletion of a given PAR protein by RNA interference (RNAi) led to reduction in the size of its corresponding domain and expansion of the complementary domain (Fig. 4, I to K). Together

these results support the existence of finite, depletable pools of PAR proteins that regulate domain size.

We propose that PAR polarity can be understood through the coupling of a PAR reaction-diffusion system with advective transport. Advective triggering of a multistable system allows for robust polarization despite spatially unrestricted diffusion of PARs in the plane of the membrane (18) and renders polarization dependent on actomyosin flows without recourse to direct binding of PAR proteins to the cortical actin meshwork (18, 20, 29). Thus, passive advection in an active and flowing medium provides a simple physical mechanism for mechanically templated pattern formation in development.
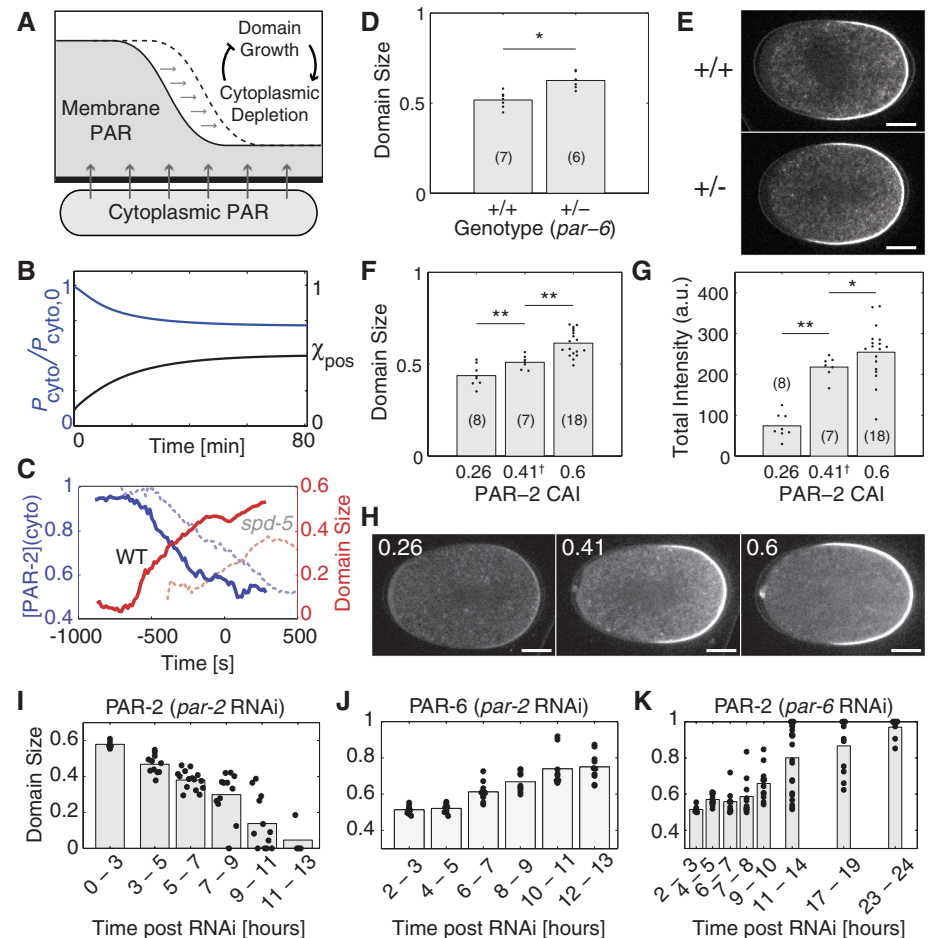
Fig. 4. Limiting pools control domain size. (**A**) Cytoplasmic depletion during domain growth inhibits further domain growth. (**B**) In the model, depletion of P_{cyto} (blue) coincides with domain growth (black, domain edge χ_{pos}). (**C**) In vivo, depletion of cytoplasmic PAR-2 (blue) coincided with domain growth (red) in WT (solid lines) and in SPD-5–depleted embryos where polarization is delayed (dashed lines). Time relative to cessation of actomyosin contractility. (**D**) PAR-2 domain size is increased in embryos with only one functional *par-6* gene copy, with (**E**) showing PAR-2 in representative embryos. +/+ embryos are homozygous WT (TH129). +/– embryos are heterozygous for *par-6* null allele *tm1425* (TH416). *$P < 0.01$, Student's t test. Number of embryos in parentheses, N. A similar effect is seen in heterozygous *par-2* strains (fig. S7). (**F**) Increasing the CAI of a *gfp::par-2* transgene resulted in increased PAR-2 domain size and, in (**G**), increased protein amounts. *$P < 0.05$, **$P < 0.01$, Welch's t test, one-tailed. (**H**) GFP::PAR-2 in CAI-adapted embryos. †For CAI = 0.41, only a central fragment was codon-optimized. (**I** and **J**) Gradual depletion of PAR-2 by RNAi leads to (I) smaller PAR-2 and (J) larger PAR-6 domains. (**K**) Depletion of PAR-6 leads to larger PAR-2 domains. Scale bars in (E) and (H) indicate 10 μm.

References and Notes

1. A. M. Turing, *Philos. Trans. R. Soc. London Ser. B* **237**, 37 (1952).
2. J. Howard, S. W. Grill, J. S. Bois, *Nat. Rev. Mol. Cell Biol.* **12**, 392 (2011).
3. J. S. Bois, F. Jülicher, S. W. Grill, *Phys. Rev. Lett.* **106**, 028103 (2011).
4. B. Etemad-Moghadam, S. Guo, K. J. Kemphues, *Cell* **83**, 743 (1995).
5. L. Boyd, S. Guo, D. Levitan, D. T. Stinchcomb, K. J. Kemphues, *Development* **122**, 3075 (1996).
6. J. L. Watts *et al.*, *Development* **122**, 3133 (1996).
7. J. Betschinger, K. Mechtler, J. A. Knoblich, *Nature* **422**, 326 (2003).
8. R. Benton, D. St. Johnston, *Cell* **115**, 691 (2003).
9. G. Tanentzapf, U. Tepass, *Nat. Cell Biol.* **5**, 46 (2003).
10. E. Munro, J. Nance, J. R. Priess, *Dev. Cell* **7**, 413 (2004).
11. A. D. Chalmers *et al.*, *Development* **132**, 977 (2005).
12. Y. Hao, L. Boyd, G. Seydoux, *Dev. Cell* **10**, 199 (2006).
13. C. Hoege *et al.*, *Curr. Biol.* **20**, 1296 (2010).
14. M. Mayer, M. Depken, J. S. Bois, F. Jülicher, S. W. Grill, *Nature* **467**, 617 (2010).
15. C. R. Cowan, A. A. Hyman, *Nature* **431**, 92 (2004).
16. A. A. Cuenca, A. Schetter, D. Aceto, K. Kemphues, G. Seydoux, *Development* **130**, 1255 (2003).
17. S. N. Hird, J. G. White, *J. Cell Biol.* **121**, 1343 (1993).
18. N. W. Goehring, C. Hoege, S. W. Grill, A. A. Hyman, *J. Cell Biol.* **193**, 583 (2011).
19. A. Jilkine, A. F. M. Marée, L. Edelstein-Keshet, *Bull. Math. Biol.* **69**, 1943 (2007).
20. F. Tostevin, M. Howard, *Biophys. J.* **95**, 4512 (2008).
21. C. A. Shelton, J. C. Carter, G. C. Ellis, B. Bowerman, *J. Cell Biol.* **146**, 439 (1999).
22. M.-C. Tsai, J. Ahringer, *J. Cell Biol.* **179**, 397 (2007).
23. S. Zonies, F. Motegi, Y. Hao, G. Seydoux, *Development* **137**, 1669 (2010).
24. Y. Mori, A. Jilkine, L. Edelstein-Keshet, *Biophys. J.* **94**, 3684 (2008).
25. A. Gamba *et al.*, *Proc. Natl. Acad. Sci. U.S.A.* **102**, 16927 (2005).
26. Y. Arai *et al.*, *Proc. Natl. Acad. Sci. U.S.A.* **107**, 12399 (2010).
27. A. Jilkine, L. Edelstein-Keshet, *PLOS Comput. Biol.* **7**, e1001121 (2011).
28. S. Redemann *et al.*, *Nat. Methods* **8**, 250 (2011).
29. D. P. Hill, S. Strome, *Dev. Biol.* **125**, 75 (1988).

Degradation of Paternal Mitochondria by Fertilization-Triggered Autophagy in *C. elegans* Embryos

Miyuki Sato and Ken Sato*

The mitochondrial genome is believed to be maternally inherited in many eukaryotes. Sperm-derived paternal mitochondria enter the oocyte cytoplasm upon fertilization and then normally disappear during early embryogenesis. However, the mechanism responsible for this clearance has been unknown. Here, we show that autophagy, which delivers cytosolic components to lysosomes for degradation, is required for the elimination of paternal mitochondria in *Caenorhabditis elegans*. Immediately after fertilization, sperm-derived components trigger the localized induction of autophagy around sperm mitochondria. Autophagosomes engulf paternal mitochondria, resulting in their lysosomal degradation during early embryogenesis. In autophagy-defective zygotes, paternal mitochondria and their genome remain even in the first larval stage. Thus, fertilization-triggered autophagy is required for selective degradation of paternal mitochondria and thereby maternal inheritance of mitochondrial DNA.

It is widely believed that mitochondrial DNA (mtDNA) is maternally inherited in many eukaryotes despite the fact that paternal mitochondria enter into the ooplasm after fertilization in most species (*1*, *2*). One possible explanation is that the paternal mtDNA is simply diluted with an excess copy number of oocyte mtDNA and hardly detected in embryos (*3*). Another is that the paternal mtDNA and mitochondria themselves are selectively degraded and eliminated from the embryonic cytoplasm. Cytologically, sperm-derived mitochondria packed in the midpiece disappear during early embryogenesis, typically by the eight-cell stage in mice (*4*). Active digestion of the paternal mtDNA in embryos was also observed (*5*, *6*). Involvement of the ubiquitin-proteasome system has been suggested in mammals (*7*); however, the mechanisms responsible for the clearance of paternal mitochondria from the embryonic cytoplasm still largely remain unknown. Macroautophagy (referred as autophagy hereafter) is another major degradation system of cytoplasmic proteins and organelles in which a portion of the cytoplasm is sequestered into autophagosomes and targeted to lysosomes (*8–11*). In mice, autophagy is essential for preimplantation development by supporting a normal rate of protein synthesis (*12*). In *Caenorhabditis elegans*, autophagy is required for dauer formation and P-granule degradation (*13*, *14*), but its function in early development had not been addressed.

In *C. elegans*, oocytes of the hermaphrodite gonad are arrested in meiotic prophase I. After the mature oocyte is ovulated and travels to the spermatheca, which contains sperm, immediate fertilization results. Subsequently, embryos move to the uterus, complete meiosis, and start zygotic development (fig. S1A) (*15*, *16*). Males can inseminate the hermaphrodites, and male sperm is predominantly used to fertilize oocytes (*17*). Worm sperm lacks a flagellum (midpiece and tail structures) but contains 50 to 70 tightly packed mitochondria around the nucleus (fig. S1B) (*18*). To monitor the fate of sperm-derived mitochondria in embryos, males were incubated in the presence of MitoTracker Red (MT) to stain sperm mitochondria and mated with nonlabeled hermaphrodites (fig. S1). The paternal condensed pronuclear DNA and MT-labeled paternal mitochondria clustering around it were detected in the very early embryo (Fig. 1A). Sperm-derived mitochondria then became scattered throughout the cytoplasm, keeping a condensed granular appearance in the pronuclear-fusion stage. These paternal MT signals gradually disappeared, and most signals were entirely undetectable by the 16-cell stage (Fig. 1, B to E). In two- and four-cell stage embryos, sperm-derived mitochondria seemed to be randomly inherited into most blastomeres. We also labeled sperm mitochondria with heat shock protein-6–GFP (green fluorescent protein; mtGFP) and observed similar results (fig. S2).

To test the possible involvement of autophagy in the degradation of sperm-derived mitochondria, we first monitored autophagosome formation in embryos that maternally express GFP–LGG-1. LGG-1 is a homolog of LC3 and Atg8 that is necessary for autophagosome formation and also serves as a marker for autophagosome membranes (*8*, *9*, *11*). In oocytes, several small GFP–LGG-1–labeled puncta were scattered throughout the cytoplasm (Fig. 2A). After fertilization, strong accumulation of GFP–LGG-1 was detected on vesicular structures clustering in one pole of the early embryos (Fig. 2B, arrow). We found that these GFP–LGG-1–positive structures were distributed around the paternal pronuclear DNA in the posterior pole region (fig. S3, C and D). The GFP–LGG-1 puncta started to disperse into the cytoplasm as the paternal pronucleus expanded (fig. S3E). The majority of GFP–LGG-1–positive puncta disappeared by the 16-cell

Laboratory of Molecular Traffic, Institute for Molecular and Cellular Regulation, Gunma University, Maebashi, Gunma 371-8512, Japan.

*To whom correspondence should be addressed. E-mail: sato-ken@gunma-u.ac.jp

Editor's Summary

Article Tools	Visit the online version of this article to access the personalization and article tools: http://science.sciencemag.org/content/334/6059/1137
Permissions	Obtain information about reproducing this article: http://www.sciencemag.org/about/permissions.dtl